Three-Dimensional Mask Transmission Simulation Using a Single Integral Equation Method

Michael S. Yeung and Eytan Barouch

Department of Manufacturing Engineering, Boston University, Boston, MA 02215

ABSTRACT

A single integral equation formulation for electromagnetic scattering from three-dimensional dielectric objects is discussed. The new formulation converges significantly faster than the traditional, coupled integral equation formulation. The new formulation is extended to incorporate the exact boundary conditions for isolated mask features by using dyadic Green's functions for the stratified medium background. Results of three-dimensional phase-shifting mask simulation are presented.

Keywords: photolithography simulation, single integral equation, dyadic Green's functions

1. INTRODUCTION

Computer simulation of photolithography has become a cost-effective way to assess the effects of scattering from wafer topography and transmission through mask apertures. With the scaling of devices to smaller dimensions, greater demands are placed on the accuracy of the physical models used in the simulators and the efficiency of their numerical implementation.

The most common technique for rigorous mask transmission simulation is the finite-difference time-domain (FDTD) method. The efficiency of FDTD on massively parallel supercomputers has been documented in the recent literature[1]. However, FDTD is much less efficient when implemented on personal computers and workstations due to the lack of massive parallelism on these platforms. Indeed, on such platforms, certain recently developed frequency-domain techniques may rival FDTD in speed. Furthermore, frequency-domain techniques are capable of yielding greater accuracy than FDTD in mask transmission problems, which often involve highly dispersive materials such as chrome. This is because highly dispersive materials are treated exactly by frequency-domain techniques without using approximate permittivity models.

In this paper, we present a new frequency-domain technique for rigorous mask transmission simulation based on the surface integral equation approach to electromagnetic scattering. In this technique, a *single* surface current unknown replaces the pair of electric and magnetic surface current unknowns used in the traditional, coupled integral equation formulation for dielectric scatterers. Our approach is based on an idea developed by D. Maystre in the late seventies for two-dimensional dielectric grating problems[2]. Our single integral equation formulation, which is discussed in Section 2, represents the first successful extension of Maystre's idea to three-dimensional problems. Numerical results for the canonical problem of a dielectric sphere, for which the exact solution is known, are presented to demonstrate the accuracy and speed of our new formulation.

In mask transmission simulation, as in nonplanar photoresist exposure simulation, one has to take into account the presence of a substrate background extending essentially to infinity horizontally. To reduce the substrate region to a manageable size, the usual approach is to truncate the computational domain by enforcing periodic boundary conditions in the horizontal plane. When the mask feature under study is an *isolated* feature, however, periodic boundary conditions cannot, strictly speaking, be employed. We have developed a new technique to simulate isolated mask features rigorously without employing periodic boundary conditions. This technique, which is discussed in Section 3, is based on dyadic Green's functions for stratified dielectric media. The computation of

0277-786X/98/$10.00

The far-zone pattern of the light transmitted through the mask using dyadic Green's functions is discussed in Section 4 and numerical results for a phase-shifting mask example are presented in Section 5.

2. THE SINGLE INTEGRAL EQUATION METHOD

The geometry of a typical mask transmission problem is illustrated in Fig. 1, which shows a 180°-phase region of an alternating phase-shifting mask structure. This region consists of a hole etched through a thin chrome layer and into a thick quartz substrate. Light is incident from the quartz side of the structure and the transmitted light on the air side is to be computed.

Examination of the structure shown in Fig. 1 reveals that it is made up of a small number of surfaces separating different *homogeneous* dielectric regions. The surface integral equation method is ideal for solving electromagnetic scattering problems involving this kind of structure. The basic idea of this method is to represent the scattered fields in each homogeneous region in terms of suitable unknown currents flowing on the surface enclosing that region. In the traditional, coupled integral equation formulation, these unknown currents are the equivalent electric and magnetic currents $\mathbf{J}_e$ and $\mathbf{J}_m$ which are related to the magnetic and electric fields $\mathbf{H}$ and $\mathbf{E}$ on the surface by

$$\mathbf{J}_e = \mathbf{n} \times \mathbf{H} , \tag{1}$$

$$\mathbf{J}_m = -\mathbf{n} \times \mathbf{E} , \tag{2}$$

where $\mathbf{n}$ is the unit normal to the surface pointing into the region under consideration. A pair of coupled integral equations for the unknown currents $\mathbf{J}_e$ and $\mathbf{J}_m$ on each surface can be derived by imposing the boundary conditions of continuity of the tangential fields across that surface. The details of this method are well known[3].

For problems of interest to us, the number of unknown current coefficients is in the range of tens of thousands. The only practical way to solve a dense matrix problem of this size is to use an iterative technique, such as the generalized minimum residual (GMRES) algorithm. However, when the traditional coupled integral equation was solved using the latter algorithm, it was found that the convergence rate of the iterative solution was very slow[4,5]. This limited the practical accuracy attainable with the coupled integral equation method to about one percent without excessively long computation times. To overcome this problem, we have developed a new, single integral equation formulation which requires half as many unknowns as the traditional formulation.

Our single integral equation (SIE) formulation is best explained by considering the simpler example of electromagnetic scattering from a finite homogeneous dielectric object embedded in an infinite homogeneous dielectric medium. Let S denote the surface of the object separating the interior region of permittivity ϵ_2 from the exterior region of permittivity ϵ_1, as illustrated in Fig. 2. Whereas in the traditional formulation the fields $\mathbf{E}^{(2)}$ and $\mathbf{H}^{(2)}$ in the interior region are expressed in terms of two surface currents flowing on S, in our SIE formulation these fields are expressed in terms of a single effective surface current $\mathbf{J}_{\text{eff}}$ flowing on S by

$$\mathbf{E}^{(2)}(\mathbf{r}) = j\omega \mathbf{A}_e^{(2)}(\mathbf{r}) - \nabla \Phi_e^{(2)}(\mathbf{r}) , \tag{3}$$

$$\mathbf{H}^{(2)}(\mathbf{r}) = \frac{1}{\mu_0} \nabla \times \mathbf{A}_e^{(2)}(\mathbf{r}) , \tag{4}$$

where

$$\mathbf{A}_e^{(2)}(\mathbf{r}) = \mu_0 \int_S G_2(\mathbf{r} - \mathbf{r}\,') \mathbf{J}_{\text{eff}}(\mathbf{r}\,')\, dS' , \tag{5}$$

$$\Phi_e^{(2)}(\mathbf{r}) = \frac{1}{j\omega\epsilon_2} \int_S G_2(\mathbf{r} - \mathbf{r}\,') \nabla' \cdot \mathbf{J}_{\text{eff}}(\mathbf{r}\,')\, dS' , \tag{6}$$

and $G_2(\mathbf{r} - \mathbf{r}\,')$ is the scalar Green's function for the interior region,

$$G_2(\mathbf{r} - \mathbf{r}\,') = \frac{e^{jk_2|\mathbf{r}-\mathbf{r}\,'|}}{4\pi|\mathbf{r} - \mathbf{r}\,'|} . \tag{7}$$

By letting the field point $\mathbf{r}$ in Eqs. (3) and (4) approach S from the interior region, we obtain the tangential fields $\mathbf{n}\times\mathbf{E}^{(2)}$ and $\mathbf{n}\times\mathbf{H}^{(2)}$ on S, where $\mathbf{n}$ is the unit normal to S pointing out of the object. By the electromagnetic equivalence principle, these tangential fields are related to the equivalent electric and magnetic currents $\mathbf{J}_e$ and $\mathbf{J}_m$ for the exterior region by

$$\mathbf{J}_e(\mathbf{r}) = \mathbf{n}\times\mathbf{H}^{(2)}(\mathbf{r}) , \tag{8}$$

$$\mathbf{J}_m(\mathbf{r}) = -\mathbf{n}\times\mathbf{E}^{(2)}(\mathbf{r}) . \tag{9}$$

The total magnetic field in the exterior region is then given by

$$\mathbf{H}^{(1)}(\mathbf{r}) = \mathbf{H}_{\text{inc}}(\mathbf{r}) + \frac{1}{\mu_0}\nabla\times\mathbf{A}_e^{(1)}(\mathbf{r}) + j\omega\mathbf{A}_m^{(1)}(\mathbf{r}) - \nabla\Phi_m^{(1)}(\mathbf{r}) , \tag{10}$$

where

$$\mathbf{A}_e^{(1)}(\mathbf{r}) = \mu_0\int_S G_1(\mathbf{r}-\mathbf{r}')\mathbf{J}_e(\mathbf{r}')\,dS' , \tag{11}$$

$$\mathbf{A}_m^{(1)}(\mathbf{r}) = \epsilon_1\int_S G_1(\mathbf{r}-\mathbf{r}')\mathbf{J}_m(\mathbf{r}')\,dS' , \tag{12}$$

$$\Phi_m^{(1)}(\mathbf{r}) = \frac{1}{j\omega\mu_0}\int_S G_1(\mathbf{r}-\mathbf{r}')\nabla'\cdot\mathbf{J}_m(\mathbf{r}')\,dS' , \tag{13}$$

and $G_1(\mathbf{r}-\mathbf{r}')$ is the scalar Green's function for the exterior region, which is given by an expression similar to Eq. (7) with the subscript 2 replaced by 1.

Notice that the equivalent currents $\mathbf{J}_e$ and $\mathbf{J}_m$ appearing in Eqs. (11) to (13), which are given by Eqs. (8) and (9), are themselves functions of the unknown effective current $\mathbf{J}_{\text{eff}}$ through Eqs. (3) to (6). A single integral equation for the effective current $\mathbf{J}_{\text{eff}}$ can be derived from Eq. (10). By letting the field point $\mathbf{r}$ in this equation approach S from the ***interior*** region, the result must be zero. Hence, our single integral equation is

$$0 = \mathbf{H}_{\text{inc}}(\mathbf{r}) + \frac{1}{\mu_0}\nabla\times\mathbf{A}_e^{(1)}(\mathbf{r}) + j\omega\mathbf{A}_m^{(1)}(\mathbf{r}) - \nabla\Phi_m^{(1)}(\mathbf{r}) . \tag{14}$$

Eq. (14) can be solved for $\mathbf{J}_{\text{eff}}$ by using the method of moments[6].

Like the coupled integral equation method, SIE is a rigorous method since it employs the exact boundary conditions on the surface S of the object and at infinity. The accuracy of the SIE method is illustrated in Fig. 3, which shows good agreement between the results of the SIE method and the exact solution for the canonical problem of a dielectric sphere illuminated by an incident plane wave. The convergence rate of the iterative solution of the SIE matrix system is also very good. This is illustrated in Fig. 4, which shows that the SIE method converged almost two orders of magnitudes faster than the coupled integral equation method for another dielectric sphere example.

3. SCATTERING IN A LAYERED MEDIUM

In the previous section, we have discussed the simple case of a single closed surface S separating two homogeneous dielectric regions, as shown in Fig. 2. In the mask transmission problem of Fig. 1, however, there are several surfaces separating several homogeneous dielectric regions, as illustrated in Fig 5. If one were to apply the integral equation formulation of the previous section straightforwardly to the structure of Fig. 5, one would have to introduce an unknown effective current flowing on the surface enclosing *each* dielectric region. Furthermore, some of the surfaces shown in Fig. 5, namely, S_2 to S_5, actually extend to infinity horizontally. On such infinite surfaces, it would in principle be necessary to introduce an infinite number of unknown current coefficients, unless the simulation domain were artificially truncated by enforcing periodic boundary conditions. In any case, the

total number of unknown current coefficients in the geometry of Fig. 5 would be very large, even though we are only interested in a small portion of the structure, namely, the etched hole in the mask.

To reduce the required number of unknown current coefficients, we have developed a *new* approach to the mask transmission problem. In this approach, the etched hole in the mask is viewed as a bubble of air buried in an otherwise uniformly stratified medium consisting of three regions: a quartz half-space above, a thin layer of chrome and an air half-space below. Powerful mathematical techniques[7,8] exist for treating the problem of electromagnetic-wave propagation in a stratified medium. These techniques are based on dyadic, or tensor, Green's functions for the stratified medium, which automatically take into account the multiple reflections occurring at the various material interfaces and the exact outgoing wave boundary conditions at infinity in *all* directions. With the exact boundary conditions in the stratified-medium *background* being taken care of by these dyadic Green's functions, we can focus our attention on the buried air bubble and introduce unknown current coefficients *only* on the surface S of the bubble, as illustrated in Fig. 6.

In the geometry shown in Fig. 6, the closed surface S separates the interior of the bubble, which is air, from the exterior, which is a stratified medium. Since the interior region is homogeneous, the discussion of Section 2 applies to this region. In particular, the fields in the interior region are still given by Eqs. (3) to (7) and the equivalent currents for the exterior region are still given by Eqs. (8) and (9). The total magnetic field in the exterior region can still be written in the form of Eq. (10). However, Eqs. (11) to (13) for the vector and scalar potentials in the exterior region must be modified, since the exterior region is now a stratified medium. The modified expressions for the vector and scalar potentials in the exterior region are

$$\mathbf{A}_e^{(1)}(\mathbf{r}) = \mu_0 \int_S \overleftrightarrow{\mathcal{G}}_E(\mathbf{r}|\mathbf{r}') \cdot \mathbf{J}_e(\mathbf{r}')\, dS' , \tag{15}$$

$$\mathbf{A}_m^{(1)}(\mathbf{r}) = \epsilon_0 \int_S \left[\overleftrightarrow{\mathcal{G}}_M(\mathbf{r}|\mathbf{r}') \cdot \mathbf{J}_m(\mathbf{r}') + \nabla C_M(\mathbf{r}|\mathbf{r}') J_{mz}(\mathbf{r}') \right] dS' , \tag{16}$$

$$\Phi_m^{(1)}(\mathbf{r}) = \frac{1}{j\omega\mu_0} \int_S K_M(\mathbf{r}|\mathbf{r}') \nabla' \cdot \mathbf{J}_m(\mathbf{r}')\, dS' , \tag{17}$$

where $\overleftrightarrow{\mathcal{G}}_E$ and $\overleftrightarrow{\mathcal{G}}_M$ are the dyadic Green's functions for the stratified-medium background, K_M is a scalar-potential Green's function and C_M is a correction term associated with the vertical component of the equivalent magnetic current. The form of the dyadic Green's functions depends on the choice of gauge. In Sommerfeld's gauge[9], the dyadic Green's functions have the form

$$\overleftrightarrow{\mathcal{G}}_E(\mathbf{r}|\mathbf{r}') = (\mathbf{xx}+\mathbf{yy}) G_{xx}^E(\mathbf{r}|\mathbf{r}') + \mathbf{zx} G_{zx}^E(\mathbf{r}|\mathbf{r}') + \mathbf{zy} G_{zy}^E(\mathbf{r}|\mathbf{r}') + \mathbf{zz} G_{zz}^E(\mathbf{r}|\mathbf{r}') , \tag{18}$$

$$\overleftrightarrow{\mathcal{G}}_M(\mathbf{r}|\mathbf{r}') = (\mathbf{xx}+\mathbf{yy}) G_{xx}^M(\mathbf{r}|\mathbf{r}') + \mathbf{zx} G_{zx}^M(\mathbf{r}|\mathbf{r}') + \mathbf{zy} G_{zy}^M(\mathbf{r}|\mathbf{r}') + \mathbf{zz} G_{zz}^M(\mathbf{r}|\mathbf{r}') . \tag{19}$$

The components of the dyadic Green's functions are expressed in the form of Sommerfeld integrals,

$$G_{xx}^E(\mathbf{r}|\mathbf{r}') = \frac{j}{2\pi\omega\mu_0} \int_0^\infty J_0(\lambda\rho)\, V_i^h(\lambda, z, z') \lambda d\lambda , \tag{20}$$

$$G_{zx}^E(\mathbf{r}|\mathbf{r}') = \frac{1}{2\pi} \frac{\partial}{\partial x} \int_0^\infty J_0(\lambda\rho) \left[I_i^h(\lambda, z, z') - I_i^e(\lambda, z, z') \right] \frac{d\lambda}{\lambda} , \tag{21}$$

$$G_{zy}^E(\mathbf{r}|\mathbf{r}') = \frac{1}{2\pi} \frac{\partial}{\partial y} \int_0^\infty J_0(\lambda\rho) \left[I_i^h(\lambda, z, z') - I_i^e(\lambda, z, z') \right] \frac{d\lambda}{\lambda} , \tag{22}$$

$$G_{zz}^E(\mathbf{r}|\mathbf{r}') = \frac{j}{2\pi\omega\epsilon(z')} \int_0^\infty J_0(\lambda\rho)\, I_v^e(\lambda, z, z') \lambda d\lambda , \tag{23}$$

$$G_{xx}^M(\mathbf{r}|\mathbf{r}') = \frac{j}{2\pi\omega\epsilon_0} \int_0^\infty J_0(\lambda\rho)\, I_v^e(\lambda, z, z') \lambda d\lambda , \tag{24}$$

$$G_{zx}^M(\mathbf{r}|\mathbf{r}') = \frac{\epsilon(z)}{2\pi\epsilon_0} \frac{\partial}{\partial x} \int_0^\infty J_0(\lambda\rho) \left[V_v^e(\lambda, z, z') - V_v^h(\lambda, z, z') \right] \frac{d\lambda}{\lambda} , \tag{25}$$

$$G^M_{zy}(\mathbf{r}|\mathbf{r}') = \frac{\epsilon(z)}{2\pi\epsilon_0}\frac{\partial}{\partial y}\int_0^\infty J_0(\lambda\rho)\,[V^e_v(\lambda,z,z') - V^h_v(\lambda,z,z')]\frac{d\lambda}{\lambda}\ , \tag{26}$$

$$G^M_{zz}(\mathbf{r}|\mathbf{r}') = \frac{j\omega\epsilon(z)}{2\pi k_0^2}\int_0^\infty J_0(\lambda\rho)\,V^h_i(\lambda,z,z')\lambda d\lambda\ . \tag{27}$$

Similarly, the scalar-potential Green's function and correction term are given by

$$K_M(\mathbf{r}|\mathbf{r}') = \frac{j\omega\mu_0}{2\pi}\int_0^\infty J_0(\lambda\rho)\,[I^e_v(\lambda,z,z') - I^h_v(\lambda,z,z')]\frac{d\lambda}{\lambda}\ , \tag{28}$$

$$C_M(\mathbf{r}|\mathbf{r}') = \frac{\epsilon(z')}{2\pi\epsilon_0}\int_0^\infty J_0(\lambda\rho)\,[I^e_i(\lambda,z,z') - I^h_i(\lambda,z,z')]\frac{d\lambda}{\lambda}\ . \tag{29}$$

In the above equations, V^h_i, V^e_i, I^e_v and I^h_v are solutions of the following telegraphist's equations with impulse sources,

$$\frac{\partial^2 V^h_i}{\partial z^2} + [\omega^2\mu_0\epsilon(z) - \lambda^2]V^h_i = j\omega\mu_0\,\delta(z-z')\ , \tag{30}$$

$$\frac{\partial^2 V^e_i}{\partial z^2} + [\omega^2\mu_0\epsilon(z) - \lambda^2]V^e_i = j\left[\frac{\omega^2\mu_0\epsilon(z) - \lambda^2}{\omega\epsilon(z)}\right]\delta(z-z')\ , \tag{31}$$

$$\frac{\partial^2 I^e_v}{\partial z^2} + [\omega^2\mu_0\epsilon(z) - \lambda^2]I^e_v = j\omega\epsilon(z)\,\delta(z-z')\ , \tag{32}$$

$$\frac{\partial^2 I^h_v}{\partial z^2} + [\omega^2\mu_0\epsilon(z) - \lambda^2]I^h_v = j\left[\frac{\omega^2\mu_0\epsilon(z) - \lambda^2}{\omega\mu_0}\right]\delta(z-z')\ , \tag{33}$$

and V^e_v, V^h_v, I^h_i and I^e_i are given in terms of these solutions by

$$V^e_v(\lambda,z,z') = \frac{1}{j\omega\epsilon(z)}\frac{\partial}{\partial z}I^e_v(\lambda,z,z')\ , \tag{34}$$

$$V^h_v(\lambda,z,z') = \left[\frac{-j\omega\mu_0}{\omega^2\mu_0\epsilon(z) - \lambda^2}\right]\frac{\partial}{\partial z}I^h_v(\lambda,z,z')\ , \tag{35}$$

$$I^h_i(\lambda,z,z') = \frac{1}{j\omega\mu_0}\frac{\partial}{\partial z}V^h_i(\lambda,z,z')\ , \tag{36}$$

$$I^e_i(\lambda,z,z') = \left[\frac{-j\omega\epsilon(z)}{\omega^2\mu_0\epsilon(z) - \lambda^2}\right]\frac{\partial}{\partial z}V^e_i(\lambda,z,z')\ . \tag{37}$$

It should be pointed out that, although the discussion in this paper is restricted to the case of a *homogeneous* chrome layer, it can easily be generalized to the case where the chrome layer has a spatially varying permittivity function $\epsilon_1(z)$ in the z-direction, as may happen when the chrome layer is extremely thin. In that case, the telegraphist's equations Eqs. (30) to (33) will have to be solved numerically.

When Eqs. (15) to (17) are substituted into Eq. (14) and the field point $\mathbf{r}$ is made to approach the surface S of the air bubble from the interior, we obtain a modified single integral equation for the mask transmission problem. This modified single integral equation can again be solved for the unknown effective current $\mathbf{J}_{\text{eff}}$ by using the method of moments.

4. THE FAR ZONE PATTERN

After obtaining the effective current $\mathbf{J}_{\text{eff}}$ by solving the single integral equation Eq. (14), the total magnetic field at an arbitrary point $\mathbf{r}$ in the exterior region can be computed using Eq. (10), where the vector and scalar potentials are given by Eqs. (15) to (17). We are mainly interested in the fields incident on the entrance pupil of

the projection optical system, which is assume to be many wavelengths away from the mask. In this far zone, the components of the dyadic Green's functions can be evaluated in closed form using the technique of asymptotic evaluation of integrals. The resulting asymptotic expressions for the geometry of Fig. 1 are

$$G^E_{xx}(\mathbf{r}|\mathbf{r}') = \frac{e^{jk_0r}}{4\pi r} e^{-jk_0 \sin\theta(x'\cos\phi + y'\sin\phi)} \cos\theta\, W_i^{\mathrm{TM}}(\theta, z') \ , \tag{38}$$

$$G^E_{zx}(\mathbf{r}|\mathbf{r}') = \frac{e^{jk_0r}}{4\pi r} e^{-jk_0 \sin\theta(x'\cos\phi + y'\sin\phi)} \csc\theta\cos\phi\ \left[W_i^{\mathrm{TE}}(\theta, z') - \cos^2\theta\, W_i^{\mathrm{TM}}(\theta, z')\right] \ , \tag{39}$$

$$G^E_{zy}(\mathbf{r}|\mathbf{r}') = \frac{e^{jk_0r}}{4\pi r} e^{-jk_0 \sin\theta(x'\cos\phi + y'\sin\phi)} \csc\theta\sin\phi\ \left[W_i^{\mathrm{TE}}(\theta, z') - \cos^2\theta\, W_i^{\mathrm{TM}}(\theta, z')\right] \ , \tag{40}$$

$$G^E_{zz}(\mathbf{r}|\mathbf{r}') = \frac{e^{jk_0r}}{4\pi r} e^{-jk_0 \sin\theta(x'\cos\phi + y'\sin\phi)} \frac{\epsilon_0}{\epsilon(z')} W_v^{\mathrm{TE}}(\theta, z') \ , \tag{41}$$

$$G^M_{xx}(\mathbf{r}|\mathbf{r}') = \frac{\epsilon(z')}{\epsilon_0} G^E_{zz}(\mathbf{r}|\mathbf{r}') \tag{42}$$

$$G^M_{zx}(\mathbf{r}|\mathbf{r}') = \frac{e^{jk_0r}}{4\pi r} e^{-jk_0 \sin\theta(x'\cos\phi + y'\sin\phi)} \cot\theta\cos\phi\ \left[W_v^{\mathrm{TM}}(\theta, z') - W_v^{\mathrm{TE}}(\theta, z')\right] \ , \tag{43}$$

$$G^M_{zy}(\mathbf{r}|\mathbf{r}') = \frac{e^{jk_0r}}{4\pi r} e^{-jk_0 \sin\theta(x'\cos\phi + y'\sin\phi)} \cot\theta\sin\phi\ \left[W_v^{\mathrm{TM}}(\theta, z') - W_v^{\mathrm{TE}}(\theta, z')\right] \ , \tag{44}$$

$$G^M_{zz}(\mathbf{r}|\mathbf{r}') = G^E_{xx}(\mathbf{r}|\mathbf{r}') \ , \tag{45}$$

where

$$W_i^{\mathrm{TM}}(\theta, z') = \frac{k_0\left(1 - R_{01}^{\mathrm{TM}}\right)}{\gamma_1\left(1 + R_{01}^{\mathrm{TM}} R_{12}^{\mathrm{TM}} e^{2j\gamma_1 d_1}\right)} \begin{cases} e^{j\gamma_1 z'} + R_{12}^{\mathrm{TM}} e^{j\gamma_1(2d_1 - z')} \ , & 0 < z' < d_1 \\ \left(1 + R_{12}^{\mathrm{TM}}\right) e^{j[\gamma_2(z' - d_1) + \gamma_1 d_1]} \ , & z' > d_1 \end{cases} \ , \tag{46}$$

$$W_i^{\mathrm{TE}}(\theta, z') = \frac{\gamma_1\epsilon_0\left(1 + R_{01}^{\mathrm{TE}}\right)}{k_0\epsilon_1\left(1 + R_{01}^{\mathrm{TE}} R_{12}^{\mathrm{TE}} e^{2j\gamma_1 d_1}\right)} \begin{cases} e^{j\gamma_1 z'} - R_{12}^{\mathrm{TE}} e^{j\gamma_1(2d_1 - z')} \ , & 0 < z' < d_1 \\ \left(1 - R_{12}^{\mathrm{TE}}\right) e^{j[\gamma_2(z' - d_1) + \gamma_1 d_1]} \ , & z' > d_1 \end{cases} \ , \tag{47}$$

$$W_v^{\mathrm{TE}}(\theta, z') = \frac{1 + R_{01}^{\mathrm{TE}}}{1 + R_{01}^{\mathrm{TE}} R_{12}^{\mathrm{TE}} e^{2j\gamma_1 d_1}} \begin{cases} e^{j\gamma_1 z'} + R_{12}^{\mathrm{TE}} e^{j\gamma_1(2d_1 - z')} \ , & 0 < z' < d_1 \\ \left(1 + R_{12}^{\mathrm{TE}}\right) e^{j[\gamma_2(z' - d_1) + \gamma_1 d_1]} \ , & z' > d_1 \end{cases} \ , \tag{48}$$

$$W_v^{\mathrm{TM}}(\theta, z') = \frac{1 - R_{01}^{\mathrm{TM}}}{1 + R_{01}^{\mathrm{TM}} R_{12}^{\mathrm{TM}} e^{2j\gamma_1 d_1}} \begin{cases} e^{j\gamma_1 z'} - R_{12}^{\mathrm{TM}} e^{j\gamma_1(2d_1 - z')} \ , & 0 < z' < d_1 \\ \left(1 - R_{12}^{\mathrm{TM}}\right) e^{j[\gamma_2(z' - d_1) + \gamma_1 d_1]} \ , & z' > d_1 \end{cases} \ . \tag{49}$$

In Eqs. (46) to (49), R_{ij}^{TE} and R_{ij}^{TM} are the TE and TM reflection coefficients at the interface between layers i and j for a ray incident from the air half-space at an angle of incidence θ, and γ_i is the z-component of the ray's wavevector in layer i. It should be pointed out that, in computing the diffraction pattern of an isolated mask feature using Eqs. (15) to (17), one has to integrate only over a *finite* surface S enclosing the corresponding air bubble. On the other hand, to compute the diffraction pattern of an isolated feature using the amended Kirchhoff-Huygens principle, namely, Eqs. (11) to (13) with the index 1 replaced by 0, one would, strictly speaking, have to integrate over an *infinite* horizontal surface situated just below the chrome layer in the geometry of Fig. 1. This is because the transmitted fields in principle extend to infinity on such a surface.

5. NUMERICAL RESULTS

We tested the above formulation on the example of a phase-shifting mask structure consisting of a square contact hole with nominal width $W = 2\lambda$ on the mask. The structure was assumed to have been formed by a

two-step etch process: a chrome etch followed by a quartz etch. The anisotropy ratio and amount of overetch for each etching step can be varied. An analytical model was used to compute the final etched profile of the structure. The surface of the etched opening was triangulated, as shown in Fig. 7, and the resulting triangular-patch model of the surface was used as input to the SIE solver.

Fig. 8 shows the far-zone diffraction pattern of the phase-shifting mask structure for a particular set of etch parameters. Notice that the diffraction pattern is a continuous function of the spatial frequency $\frac{\sin\theta}{\lambda}$, rather than a discrete set of impulse functions representing various diffraction orders. This is because our formulation based on dyadic Green's functions does *not* employ any periodic boundary conditions. Hence, the spectrum of the light transmitted through the isolated contact hole should be a continuous function of the spatial frequency. The diffraction pattern shown in Fig. 8 has a form resembling the $\frac{1}{2}(1+\cos\theta)\,\mathrm{sinc}\left(\frac{k_0 W}{2}\sin\theta\right)$ function given by the scalar diffraction theory for an isolated contact hole.

6. CONCLUSIONS

We have presented a single integral equation formulation for electromagnetic scattering from three-dimensional dielectric objects in which a single unknown surface current appears. We have also discussed how the exact boundary conditions for isolated mask features can be incorporated into the formulation by using dyadic Green's functions. As a result, we have been able to simulate the fields transmitted through an *isolate* mask feature rigorously without the use of periodic boundary conditions. Our exact boundary conditions for isolated features will also be useful for simulating the effects of isolated or random defects on the bottom and sidewalls of a mask aperture, since periodic boundary conditions are not strictly valid for this kind of defects.

ACKNOWLEDGEMENT

This research was supported by AFOSR/DARPA MURI grant no. 97-1-0525.

REFERENCES

1. A. K. Wong and A. R. Neureuther, "Massively parallel electromagnetic simulation for photolithographic applications", *IEEE Trans. Computer-Aided Design*, Vol. CAD-14, pp. 1231-1240 (1995).
2. D. Maystre, "Integral Methods", in "Electromagnetic Theory of Gratings", R. Petit, Ed. (Springer-Verlag, 1980).
3. K. Umashankar, A. Taflove and S. M. Rao, "Electromagnetic scattering by arbitrary shaped three-dimensional homogeneous lossy dielectric objects", *IEEE Trans. Antennas Propagat.*, Vol. AP-34, pp. 758-766 (1986).
4. M. S. Yeung and E. Barouch, "Three-dimensional nonplanar lithography simulation using a periodic fast multipole method", *Proc. SPIE*, Vol. 3051, pp. 509-521 (1997).
5. M. S. Yeung and E. Barouch, "Optimization of BARC for nonplanar lithography by three-dimensional electromagnetic simulation", *Proc. SPIE*, Vol. 3183, pp. 91-103 (1997).
6. M. S. Yeung, "Single integral equation for electromagnetic scattering from three-dimensional dielectric objects" (submitted for publication).
7. J. R. Wait, "Electromagnetic Waves in Stratified Media" (Pergamon Press, New York, 1970).
8. P. E. Wannamaker, G. W. Hohmann and W. A. SanFilipo, "Electromagnetic modeling of three-dimensional bodies in layered earths using integral equations", *Geophysics*, Vol. 49, pp. 60-74 (1984).
9. A. Sommerfeld, "Partial Differential Equations in Physics" (Academic Press, New York, 1949).

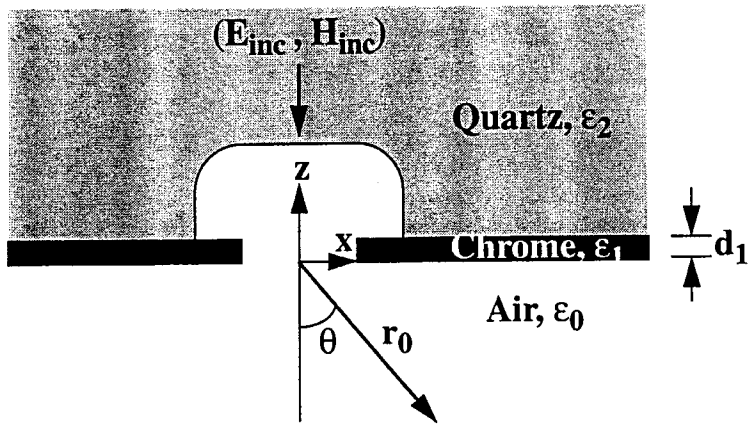

Fig. 1. Phase-shifting mask structure for mask transmission simulation. The refractive indices of quartz and chrome at $\lambda = 0.248$ μm were taken to be 1.508+0j and 0.85+2.01j, respectively.

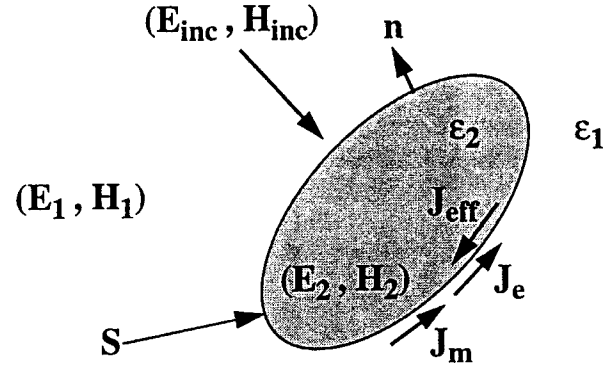

Fig. 2. Homogeneous dielectric object ε_2 in a homogeneous medium ε_1. $\mathbf{J_e}$ and $\mathbf{J_m}$ are the equivalent currents for the exterior region. $\mathbf{J_{eff}}$ is an effective current for the interior region.

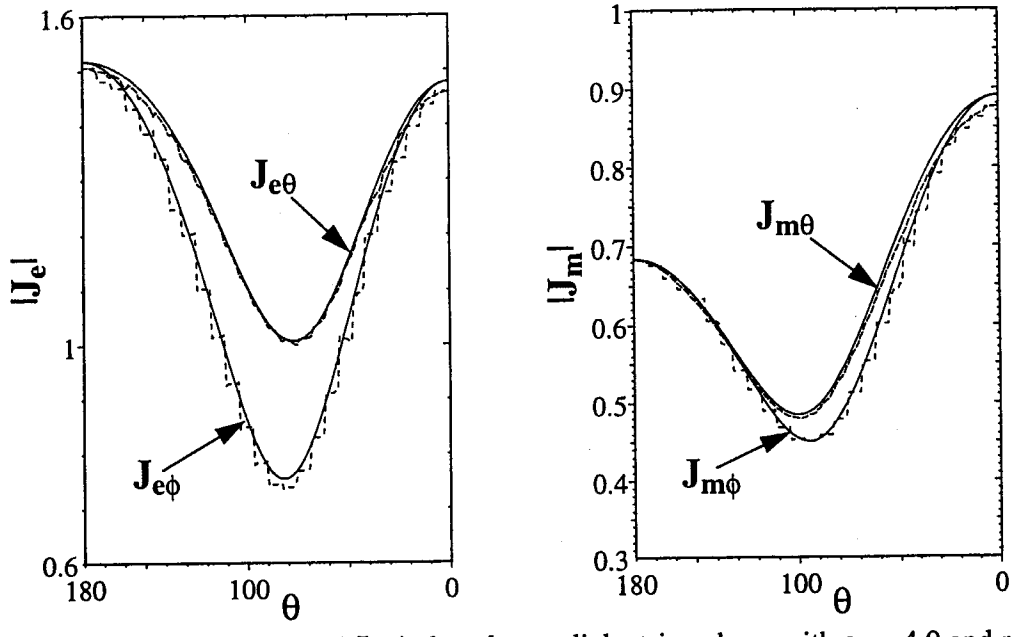

Fig. 3. Equivalent currents $\mathbf{J_e}$ and $\mathbf{J_m}$ induced on a dielectric sphere with $\varepsilon_2 = 4.0$ and radius $= 0.16\lambda$. Solid lines are the exact results. Dashed lines are the results of the SIE method.

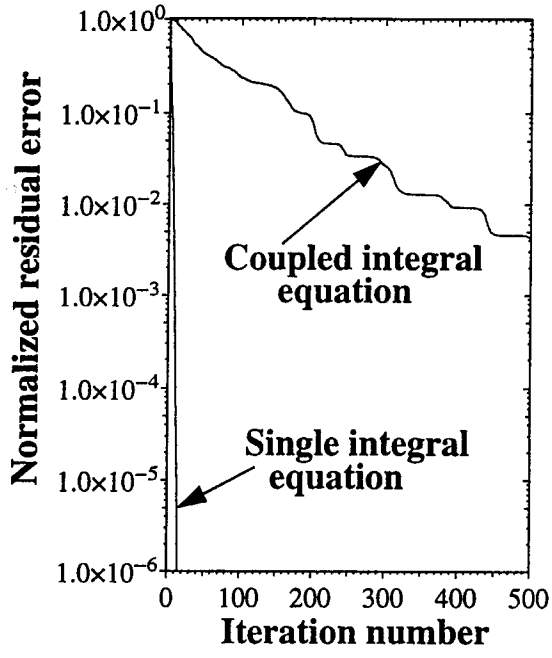

Fig. 4. Convergence rates of the single and coupled integral equation formulations for a dielectric sphere with $\varepsilon_2 = 4.0$ and radius = 0.08λ.

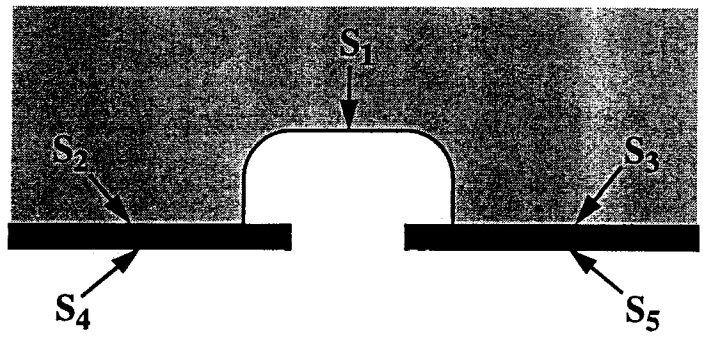

Fig. 5. Surfaces separating various dielectric regions. In integral equation formulations employing *scalar* Green's functions, one unknown effective current is needed for *each* of these surfaces.

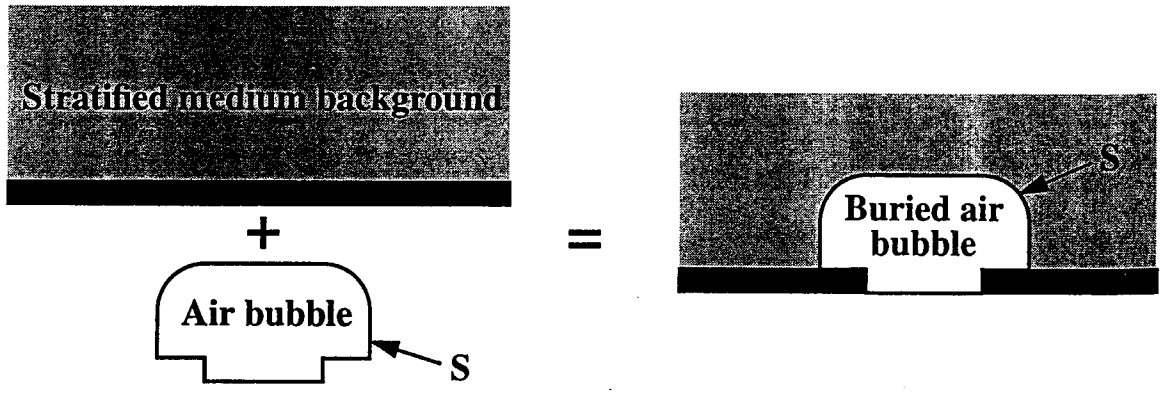

Fig. 6. The mask transmission problem viewed as an air bubble buried in a stratified medium background. By employing *dyadic* Green's functions for the stratified medium background, only the surface *S* of the bubble carries an unknown effective current.

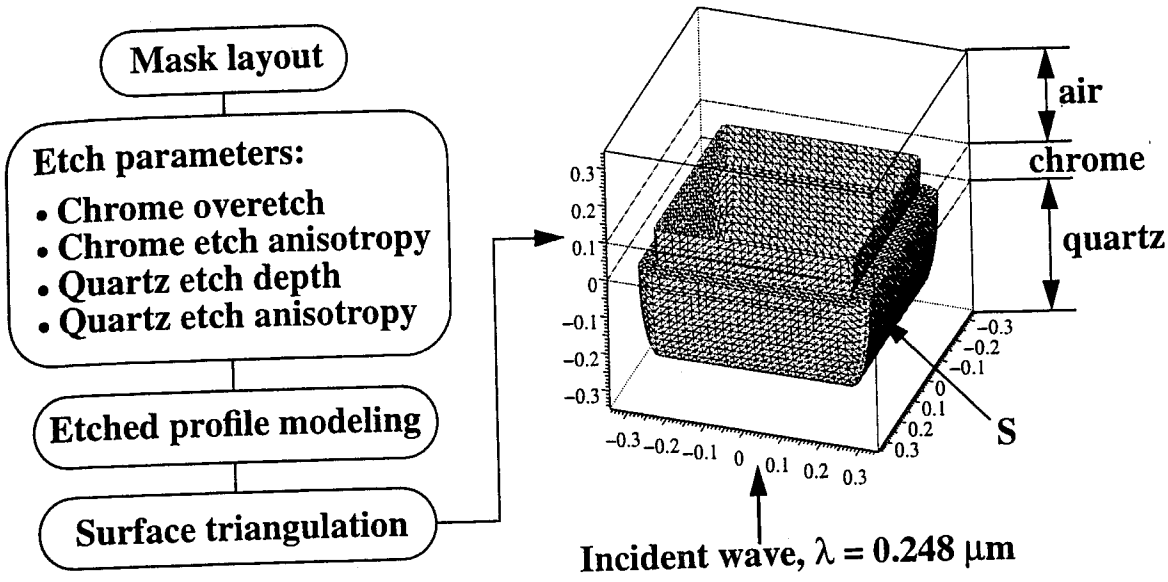

Fig. 7. Steps used in the generation of an accurate surface representation of a 180°-phase contact hole in a 4X alternating phase-shifting mask. The etched hole, viewed as an air bubble, is shown chrome-side up, with the uppermost part of its enclosing surface S removed for clarity. The thickness of the chrome was $d_1 = 0.1$ μm. The phase of the incident wave was taken to be zero at the quartz-chrome interface.

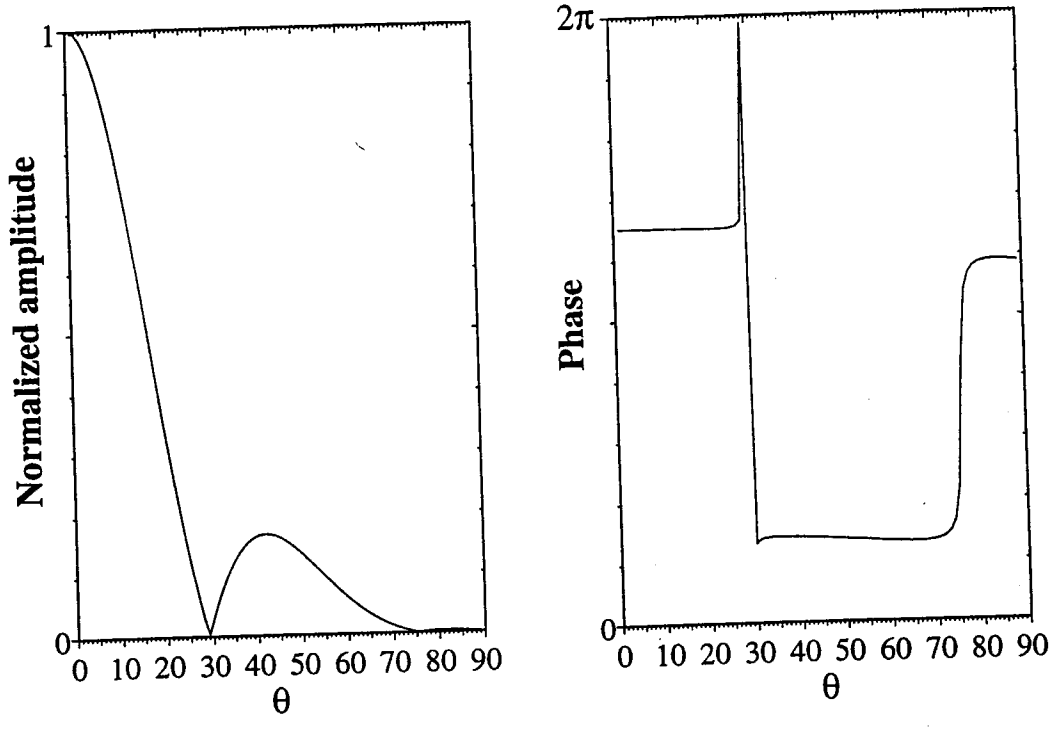

Fig. 8. Far-zone pattern of the light transmitted through the isolated contact hole shown in Fig. 7. The first minimum occurs at θ = 29° because the final etched dimension of the mask aperture was $W = 2.08\lambda$.